

J/ψ -meson photoproduction off the nucleon in a dynamical model

Sang-Ho Kim

^aDepartment of Physics and Origin of Matter and Evolution of Galaxies (OMEG) Institute, Soongsil University, , Seoul, 06978, , Republic of Korea

Abstract

The photoproduction of J/ψ meson off the nucleon is investigated within a dynamical model approach based on a Hamiltonian which describes the reaction mechanisms of the Pomeron exchange, meson exchange, and direct J/ψ radiation terms. To shed light on the low-energy mechanism, we scrutinize the role of light-meson [$\pi^0(135)$, $\eta(548)$, $\eta'(958)$, $f_1(1285)$] and charmonium-meson [$\eta_c(1S)$, $\chi_{c0}(1P)$, $\chi_{c1}(1P)$, $\eta_c(2S)$, $\chi_{c1}(3872)$] exchanges in the t -channel diagram. The values of the coupling constants are mostly determined by the radiative decays of the J/ψ meson or the relevant charmonium mesons. The final J/ψ - N interaction is required by the unitarity condition and is described by the gluon-exchange and direct $J/\psi N$ coupling terms. The parameters of the Hamiltonian are determined by the latest GlueX and J/ψ -007 experiments at the Jefferson Laboratory (JLab). We find that $\eta(548)$ and $\eta'(958)$ light mesons give the most significant contribution to $\gamma p \rightarrow J/\psi p$ among the meson-exchange terms. Meanwhile, the effect of charmonium mesons turns out to be small compared to that of light mesons. It turns out that the contribution of the FSI term is about 1 - 2 orders of magnitude smaller than that of the Born term and is significant near the threshold when the Yukawa form is used as for the charmonium-nucleon potential. The resulting total and t -dependent differential cross sections provide good agreement with the JLab data. The angle-dependent data with high precision near the very threshold ($E_\gamma \leq 8.9$ GeV) are strongly desired to pin down the role of the FSI term more properly.

Keywords: J/ψ photoproduction, Pomeron exchange, meson exchanges, final state interactions

1. Introduction

It is well known that the photoproduction of light vector mesons (ρ , ω , and ϕ) and J/ψ meson off the nucleon at high energies are governed by the diffractive processes and are described by the t -channel Pomeron exchange. In case of the production of light vector mesons, the slowly rising cross sections with the beam energy W is verified by the soft Pomeron exchange with its trajectory $\alpha_{\mathbb{P}}(t) = 1.08 + 0.25t$ [1]. Meanwhile, the measurements for J/ψ meson reveal a steeper dependence on W than expected from the universal soft Pomeron exchange. To account for the FermiLab [2, 3], ZEUS [4], and H1 [5, 6] data in the region $W \geq 10$ GeV, additional hard Pomeron exchange is suggested by Donnachie and Landshoff (DL) [7, 8, 9, 10].

Other reaction models for $\gamma p \rightarrow J/\psi p$ [11] involve the two- and three-gluon exchanges based on perturbative quantum chromodynamics (pQCD) and effective heavy quark field theory [12], the pQCD approach to calculate the two-gluon exchange using the generalized parton distribution (GPD) of the nucleon [13], the exchanges of scalar (0^{++}) and tensor (2^{++}) glueballs within the holographic formulation [14, 15], etc. The possibility of the existence of the s -channel hidden-charm pentaquark states P_c is also studied [16, 17, 18, 19, 20, 21, 22, 23] since it was reported by the LHCb Collaboration in the $\Lambda_b^0 \rightarrow J/\psi K^- p$ decay [24, 25].

The author and his collaborators recently studied photo- and electroproduction of ϕ meson within an effective Lagrangian approach [26, 27, 28, 29] and found that some t -channel

light mesons, such as $\pi^0(135)$, $\eta(548)$, $a_0(980)$, $f_0(980)$, and $f_1(1285)$, play a crucial role in describing the CEBAF Large Acceptance Spectrometer (CLAS) [30, 31, 32, 33] and Laser Electron Photon Experiments at SPring-8 (LEPS) [34] data at low energies $2 \leq W \leq 3$ GeV although they are expected to be suppressed due to the Okubo-Zweig-Iizuka (OZI) rule [35, 36, 37].

A different situation occurs in case of the J/ψ -photoproduction mechanism. The radiative decays of J/ψ meson mostly proceed by producing multi-mesonic resonant or non-resonant states. Its radiative decays to the π^0 and η mesons are about an order of magnitude smaller than those of ϕ meson [38]. Instead, as the mass scale increases, some charmonium mesons, such as $\chi_{c0}(1P)$ and $\chi_{c1}(1P)$, have a large product of branching ratios to the $J/\psi\gamma$ channel [38] indicating that their exchanges could give non-negligible contributions to the t -channel diagram.

In this letter, we extend our previous work for the ϕ photoproduction [28, 29] to the production of J/ψ meson within the Hamiltonian formulation [39, 40]. We construct a model Hamiltonian with the parameters determined by the recent Jefferson Laboratory (JLab) data of J/ψ photoproduction off the nucleon [41, 42, 43]. We follow the DL model [44, 45, 46] for the description of Pomeron exchange at high energies. In the low-energy region, i.e., $4 \leq W \leq 5$ GeV, we elaborate on each contribution of light mesons [$\pi^0(135)$, $\eta(548)$, $\eta'(958)$, $f_1(1285)$] and charmonium mesons [$\eta_c(1S)$, $\chi_{c0}(1P)$, $\chi_{c1}(1P)$, $\eta_c(2S)$, $\chi_{c1}(3872)$] in the t channel. The direct J/ψ radiations from the nucleon are also considered in the s - and u -channels.

The unitarity condition requires the $\gamma N \rightarrow J/\psi N$ amplitude to include the $J/\psi N \rightarrow J/\psi N$ final-state interaction (FSI) as well. The $J/\psi N \rightarrow J/\psi N$ reaction is essential for exploring the possible J/ψ -nucleus bound states predicted by lattice QCD (LQCD) calculations [47]. As for the possible sources of the $J/\psi N$ interaction, we consider the gluon-exchange mechanism within QCD and the direct $J/\psi N$ coupling amplitudes.

In the next section, we explain the general formalism of our dynamical model of J/ψ photoproduction off the nucleon. In sections 3 and 4, the formalism of the Born and FSI terms is explained, respectively, in detail. In section 5, we present the numerical results for the total and t -dependent differential cross sections and discuss them in comparison with the higher-statistics JLab data. Section 6 is devoted to summary and conclusion.

2. Dynamical model of the $\gamma p \rightarrow J/\psi p$ reaction

We can define a model Hamiltonian which can generate the $\gamma N \rightarrow J/\psi N$ reaction and $J/\psi N \rightarrow J/\psi N$ FSI term following the dynamical formulation [39, 40]

$$H = H_0 + B_{J/\psi N, \gamma N} + \Gamma_{N^*, \gamma N} + \Gamma_{N^*, J/\psi N}, \quad (1)$$

where H_0 is the free Hamiltonian of the system and $B_{J/\psi N, \gamma N}$ is the Born amplitude consisting of the tree diagrams for $\gamma N \leftrightarrow J/\psi N$. The last two terms indicate the nucleon resonance (N^*) contribution in the s channel [16, 17, 18, 19, 20, 21, 22, 23] and are not considered in this letter.

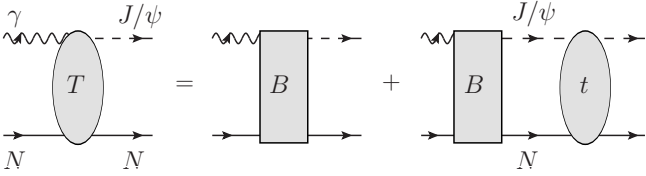


Figure 1: Full amplitude for the $\gamma N \rightarrow J/\psi N$ reaction: B is the Born amplitude and t is the $J/\psi N \rightarrow J/\psi N$ scattering amplitude.

The full amplitude for $\gamma N \rightarrow J/\psi N$ defined by the Hamiltonian of Eq. (1) is illustrated in Fig. 1 and can be written as

$$T_{J/\psi N, \gamma N}(E) = B_{J/\psi N, \gamma N} + T_{J/\psi N, \gamma N}^{\text{FSI}}, \quad (2)$$

where the last term denotes the $J/\psi N$ FSI amplitude and can be expressed as

$$T_{J/\psi N, \gamma N}^{\text{FSI}}(E) = t_{J/\psi N, J/\psi N}(E) G_{J/\psi N}(E) B_{J/\psi N, \gamma N}. \quad (3)$$

Here the meson-baryon propagator is given by

$$G_{MB}(E) = \frac{|MB\rangle\langle MB|}{E - H_0 + i\epsilon}, \quad (4)$$

and the $J/\psi N \rightarrow J/\psi N$ scattering amplitude is defined by

$$\begin{aligned} t_{J/\psi N, J/\psi N}(E) \\ = V_{J/\psi N, J/\psi N}(E) + V_{J/\psi N, J/\psi N}(E) G_{J/\psi N}(E) t_{J/\psi N, J/\psi N}(E), \end{aligned} \quad (5)$$

where the $J/\psi N$ potential is decomposed into

$$V_{J/\psi N, J/\psi N}(E) = v_{J/\psi N, J/\psi N}^{\text{Gluon}}(E) + v_{J/\psi N, J/\psi N}^{\text{Direct}}(E), \quad (6)$$

as illustrated in Fig. 2. Here $v_{J/\psi N, J/\psi N}^{\text{Gluon}}$ indicates the gluon-exchange interaction [Fig. 2(a)] and $v_{J/\psi N, J/\psi N}^{\text{Direct}}$ the direct $J/\psi N$ coupling term [Figs. 2(b,c)].

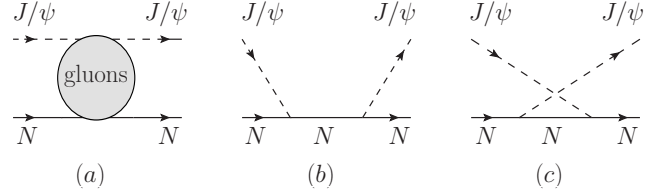


Figure 2: $J/\psi N \rightarrow J/\psi N$ scattering amplitudes: (a) gluon-exchange within QCD, (b,c) direct $J/\psi N$ coupling terms.

With the normalization condition $\langle \mathbf{k} | \mathbf{k}' \rangle = \delta^3(\mathbf{k} - \mathbf{k}')$ for plane wave states [48] and $\langle \psi_B | \psi_B \rangle = 1$ for a single particle state ψ_B , the differential cross section of

$$\gamma(q, \lambda_\gamma) + N(p_i, m_s) \rightarrow J/\psi(k, \lambda_{J/\psi}) + N(p_f, m'_s), \quad (7)$$

in the center of mass (c.m.) frame, can be written as

$$\begin{aligned} \frac{d\sigma}{d\Omega} = & \frac{(2\pi)^4}{q^2} \rho_{J/\psi N}(W) \rho_{\gamma N}(W) \frac{1}{4} \sum_{\lambda_{J/\psi}, m'_s} \sum_{\lambda_\gamma, m_s} \\ & \times |\langle k \lambda_{J/\psi}; p_f m'_s | T_{J/\psi N, \gamma N}(W) | q \lambda_\gamma; p_i m_s \rangle|^2, \end{aligned} \quad (8)$$

where

$$\rho_{J/\psi N} = \frac{k E_{J/\psi}(\mathbf{k}) E_N(\mathbf{k})}{W}, \quad \rho_{\gamma N} = \frac{q^2 E_N(\mathbf{q})}{W}, \quad (9)$$

with $\mathbf{p}_i = -\mathbf{q}$ and $\mathbf{p}_f = -\mathbf{k}$. The invariant mass is given by $W = q + E_N(\mathbf{q}) = E_{J/\psi}(\mathbf{k}) + E_N(\mathbf{k})$. λ_γ and $\lambda_{J/\psi}$ are the helicities of the photon and J/ψ meson, respectively, and m_s and m'_s are the magnetic quantum numbers of the initial and final nucleons, respectively.

3. Born term

The Feynman diagrams of the Born term for $\gamma p \rightarrow J/\psi p$ are drawn in Fig. 3, which include the exchanges of the (a) Pomeron, (b) light mesons, (c) charmonium mesons in the t channel, and (d, e) direct J/ψ radiations in the s - and u -channels. The scattering amplitude for the Born term reads

$$\begin{aligned} & \langle k \lambda_{J/\psi}; p_f m'_s | B_{J/\psi N, \gamma N} | q \lambda_\gamma; p_i m_s \rangle \\ = & \frac{1}{(2\pi)^3} \sqrt{\frac{M_N^2}{4E_{J/\psi}(\mathbf{k})E_N(\mathbf{p}_f)|\mathbf{q}|E_N(\mathbf{p}_i)}} \\ & \times [\bar{u}_N(p_f, m'_s) \mathcal{M}^{\mu\nu}(k, p_f, q, p_i) u_N(p_i, m_s)] \\ & \times \epsilon_\nu^*(k, \lambda_{J/\psi}) \epsilon_\mu(q, \lambda_\gamma), \end{aligned} \quad (10)$$

where $\epsilon_\mu(q, \lambda_\gamma)$ is the photon polarization vector with momentum q and helicity λ_γ , and $\epsilon_\nu(k, \lambda_{J/\psi})$ is that of the J/ψ meson

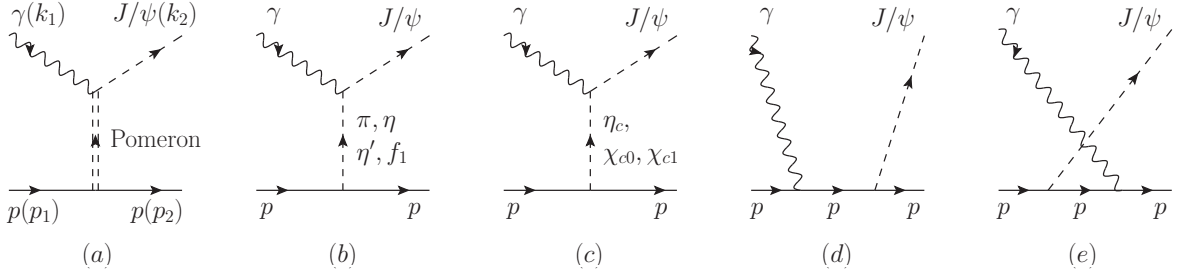


Figure 3: Born diagrams for $\gamma(q) + p(p_i) \rightarrow J/\psi(k) + p(p_f)$, which include the exchanges of (a) Pomeron, (b) light mesons [$\pi^0, \eta, \eta', f_1(1285)$], (c) charmonium mesons [$\eta_c(1S), \chi_{c0}(1P), \chi_{c1}(1P), \eta_c(2S), \chi_{c1}(3872)$] in the t channel, (d, e) direct J/ψ radiation terms in the s - and u -channels.

with momentum k and helicity $\lambda_{J/\psi}$. The nucleon spinor of momentum p and spin projection m_s is given by $u_N(p, m_s)$, which is normalized as $\bar{u}_N(p, m_s)u_N(p, m'_s) = \delta_{m_s, m'_s}$. $E_{J/\psi}$ and E_N are the energies of the J/ψ meson and nucleon, respectively. Each term of Fig. 3 will be explained in detail below.

3.1. Pomeron exchange

In the DL model [44, 45, 46], the two-gluon exchange mechanism is parametrized as the soft Pomeron exchange within the Regge phenomenology [Fig. 3(a)]. The scattering amplitude takes the form

$$\mathcal{M}_{\mathbb{P}}^{\mu\nu} = i \frac{12eM_V^2}{f_V} \beta_{qV} F_V(t) \beta_{u/d} F_N(t) [q^\mu q^\nu - \gamma^\mu q^\nu] G_{\mathbb{P}}(s, t), \quad (11)$$

where M_h is the mass of a hadron h . β_{qV} ($\beta_{u/d}$) indicates the coupling between the Pomeron and the quark in a vector meson V (nucleon N) and is determined by fitting to the cross section data of the diffractive photoproduction of vector mesons:

$$\beta_{u/d} = 2.07, \quad \beta_s = 1.39, \quad \beta_c = 0.323 \text{ [GeV}^{-1}\text{]}. \quad (12)$$

To get the vector meson decay constant f_V , we recall that the vector meson dominance (VMD) is defined by the effective Lagrangian of

$$\mathcal{L}_{\text{VMD}} = \frac{eM_V^2}{f_V} A^\mu V_\mu, \quad (13)$$

where A^μ and V_μ are the fields of the photon and vector meson, respectively. Then, f_V can be calculated from the experimental data of the width of $V \rightarrow e^+e^-$ [38] and

$$\Gamma_{V \rightarrow e^+e^-} = \alpha^2 \frac{4\pi M_V}{3 f_V^2}, \quad (14)$$

where $\alpha = e^2/(4\pi)$ with e being the unit electric charge. We finally obtain

$$\begin{aligned} f_\rho &= 4.94, & f_\omega &= 17.06, \\ f_\phi &= 13.38, & f_{J/\psi} &= 11.18, & f_\Upsilon &= 39.68. \end{aligned} \quad (15)$$

The propagator $G_{\mathbb{P}}$ in Eq. (11) is an important ingredient of the Regge phenomenology and takes the form

$$G_{\mathbb{P}}(s, t) = \left(\frac{s}{s_{\mathbb{P}}} \right)^{\alpha_{\mathbb{P}}(t)-1} \exp \left\{ -\frac{i\pi}{2} [\alpha_{\mathbb{P}}(t) - 1] \right\}. \quad (16)$$

The Pomeron trajectory is determined to be $\alpha_{\mathbb{P}}(t) = 1.25 + 0.25t$ and the mass scale is given by $s_{\mathbb{P}} = 1/\alpha'_{\mathbb{P}} = 4 \text{ GeV}^2$. The form factor for the Pomeron-vector meson vertex and the isoscalar electromagnetic (EM) form factor of the nucleon are, respectively, defined by

$$F_V(t) = \frac{2\mu_0^2}{(M_V^2 - t)(2\mu_0^2 + M_V^2 - t)}, \quad (17)$$

$$F_N(t) = \frac{4M_N^2 - 2.8t}{(4M_N^2 - t)(1 - t/0.71)^2}, \quad (18)$$

where $\mu_0 = 1.1 \text{ GeV}^2$ and $t = (q - k)^2$.

3.2. Light-meson exchanges

First, in case of light-meson exchanges [Fig. 3(b)], we consider (π, η, η') pseudoscalar mesons and $f_1(1285)$ axial-vector meson into which the radiative decays of J/ψ are non-negligible as shown in Table. 1.

The effective Lagrangians for the EM interaction read

$$\mathcal{L}_{\gamma\Phi J/\psi} = \frac{eg_{\gamma\Phi J/\psi}}{M_{J/\psi}} \epsilon^{\mu\nu\alpha\beta} \partial_\mu A_\nu \partial_\alpha \psi_\beta \Phi, \quad (19)$$

$$\mathcal{L}_{\gamma A_1 J/\psi} = \frac{eg_{\gamma A_1 J/\psi}}{M_{J/\psi}^2} \epsilon^{\mu\nu\alpha\beta} \partial_\mu A_\nu \partial^\delta \partial_\delta \psi_\alpha A_{1\beta}, \quad (20)$$

where Φ, ψ_β , and $A_{1\beta}$ are the fields of the pseudoscalar, J/ψ , and axial-vector mesons, respectively. The coupling constants are calculated from the widths of the $J/\psi \rightarrow \Phi\gamma$ and $J/\psi \rightarrow A_1\gamma$ radiative decays

$$\Gamma_{J/\psi \rightarrow \Phi\gamma} = \frac{e^2}{12\pi} \frac{q_\gamma^3}{M_{J/\psi}^2} g_{\gamma\Phi J/\psi}^2, \quad (21)$$

$$\Gamma_{J/\psi \rightarrow A_1\gamma} = \frac{e^2}{12\pi} \frac{M_{J/\psi}^2 + M_{A_1}^2}{M_{J/\psi}^2 M_{A_1}^2} q_\gamma^3 g_{\gamma A_1 J/\psi}^2, \quad (22)$$

where $q_\gamma = (M_{J/\psi}^2 - M_{\Phi, A_1}^2)/(2M_{J/\psi})$. The decay width of J/ψ is given by $\Gamma_{J/\psi} = 92.6 \text{ KeV}$.

The strong interaction Lagrangians are written as

$$\mathcal{L}_{\Phi NN} = -ig_{\Phi NN} \bar{N} \Phi \gamma_5 N, \quad (23)$$

$$\mathcal{L}_{A_1 NN} = -g_{A_1 NN} \bar{N} \left[\gamma_\mu - i \frac{K_{A_1 NN}}{2M_N} \gamma_\nu \gamma_\mu \partial^\nu \right] A_1^\mu \gamma_5 N, \quad (24)$$

Mesons (M)	Mass (J^P)	Γ_M [MeV]	$\text{Br}_{J/\psi \rightarrow M\gamma}$ [%]	$ g_{\gamma MJ/\psi} $	g_{MNN}
π	134 (0^-)	-	$(3.39 \pm 0.08) \cdot 10^{-3}$	$1.83 \cdot 10^{-3}$	13.0
η	548 (0^-)	$1.31 \cdot 10^{-3}$	$(1.090 \pm 0.013) \cdot 10^{-1}$	$1.09 \cdot 10^{-2}$	6.34
η'	958 (0^-)	0.188	$(5.28 \pm 0.06) \cdot 10^{-1}$	$2.65 \cdot 10^{-2}$	6.87
f_1	1285 (1^+)	23.0	$(6.1 \pm 0.8) \cdot 10^{-2}$	$3.93 \cdot 10^{-3}$	2.5
$\eta_c(1S)$	2984 (0^-)	30.5	1.41 ± 0.14	1.95	-

Table 1: Radiative decays of J/ψ into the light mesons and $\eta_c(1S)$ [38] and strong coupling constants g_{MNN} [49, 50].

Mesons (M)	Mass (J^P)	Γ_M [MeV]	$\text{Br}_{M \rightarrow J/\psi\gamma}$ [%]	$ g_{\gamma MJ/\psi} $	$\text{Br}_{M \rightarrow p\bar{p}}$ [%]	$ g_{Mpp} $
$\eta_c(1S)$	2984 (0^-)	30.5	-	-	$(1.33 \pm 0.11) \cdot 10^{-1}$	$2.70 \cdot 10^{-2}$
$\chi_{c0}(1P)$	3414 (0^+)	10.7	1.41 ± 0.09	1.33	$(2.21 \pm 0.14) \cdot 10^{-2}$	$4.56 \cdot 10^{-3}$
$\chi_{c1}(1P)$	3511 (1^+)	0.84	34.3 ± 1.3	3.29	$(7.6 \pm 0.4) \cdot 10^{-3}$	$8.42 \cdot 10^{-4}$
$\eta_c(2S)$	3638 (0^-)	11.8	< 1.4	< 1.32	$< 2.0 \cdot 10^{-1}$	$< 1.61 \cdot 10^{-2}$
$\chi_{c1}(3872)$	3872 (1^+)	1.19	0.78 ± 0.29	0.257	$< 2.2 \cdot 10^{-3}$	$< 5.11 \cdot 10^{-4}$

Table 2: Radiative decays of the charmonium mesons into J/ψ and strong coupling constants g_{Mpp} [38].

where $g_{\Phi NN}$ is obtained using the Nijmegen potentials [49, 50]. $g_{f_1 NN}$ is taken from Refs. [51, 52] and the tensor term $\kappa_{f_1 NN}$ is set to be zero for brevity. We summarize all the relevant parameters in Table 1.

3.3. Charmonium-meson exchanges

Second, in case of charmonium-meson exchanges, [Fig. 3(c)], we consider $\eta_c(1S)$, $\chi_{c0}(1P)$, and $\chi_{c1}(1P)$ mesons. $\eta_c(2S)$ and $\chi_{c1}(3872)$ mesons also give sizable upper limits for their branching ratios to $J/\psi\gamma$ or $p\bar{p}$. Thus we test their contributions as well.

For the exchange of $\chi_{c0}(1P)$ scalar meson, the EM interaction can be expressed by the following effective Lagrangian

$$\mathcal{L}_{\gamma S J/\psi} = \frac{e g_{\gamma S J/\psi}}{M_{J/\psi}} F^{\mu\nu} \psi_{\mu\nu} S, \quad (25)$$

where S is the field of the scalar meson. $F^{\mu\nu}$ and $\psi_{\mu\nu}$ are the EM and J/ψ field-strength tensors, respectively: $F^{\mu\nu} = \partial^\mu A^\nu - \partial^\nu A^\mu$ and $\psi_{\mu\nu} = \partial_\mu \psi_\nu - \partial_\nu \psi_\mu$. $g_{\gamma S J/\psi}$ can be obtained from the radiative decay width of $S \rightarrow J/\psi\gamma$

$$\Gamma_{S \rightarrow J/\psi\gamma} = \frac{e^2}{\pi} \frac{q_\gamma^3}{M_{J/\psi}^2} g_{\gamma S J/\psi}^2, \quad (26)$$

where $q_\gamma = (M_S^2 - M_{J/\psi}^2)/(2M_S)$.

When $\eta_c(1S)$ pseudoscalar exchanges is considered, we use the same formulae of Eq. (19) and (21) because of $M_{J/\psi} > M_{\eta_c(1S)}$. For the exchanges of $\eta_c(2S)$ pseudoscalar and [$\chi_{c1}(1P)$, $\chi_{c1}(3872)$] axial-vector mesons, the effective Lagrangians are the same as for those of Eqs. (19) and (20), respectively. The coupling constants are also obtained from the radiative decays of $\Phi \rightarrow J/\psi\gamma$ and $A_1 \rightarrow J/\psi\gamma$, the formula of which are given by

$$\Gamma_{\Phi \rightarrow J/\psi\gamma} = \frac{e^2}{3\pi} \frac{q_\gamma^3}{M_{J/\psi}^2} g_{\gamma\Phi J/\psi}^2, \quad (27)$$

$$\Gamma_{A_1 \rightarrow J/\psi\gamma} = \frac{e^2}{12\pi} \frac{M_{J/\psi}^2 + M_{A_1}^2}{M_{J/\psi}^2 M_{A_1}^2} q_\gamma^3 g_{\gamma A_1 J/\psi}^2, \quad (28)$$

where $q_\gamma = (M_{\Phi, A_1}^2 - M_{J/\psi}^2)/(2M_{\Phi, A_1})$.

The effective Lagrangian of the scalar meson with the nucleon takes the form

$$\mathcal{L}_{SNN} = -g_{SNN} \bar{N} S N. \quad (29)$$

The decays of the relevant charmonium mesons into $p\bar{p}$ are known experimentally [38]. Thus the strong coupling constants for the exchanges of the pseudoscalar, axial-vector, and scalar charmonium mesons are obtained from their decays into $p\bar{p}$

$$\Gamma_{\Phi \rightarrow p\bar{p}} = \frac{1}{\pi} \frac{q_N^3}{M_\Phi^2} g_{\Phi pp}^2, \quad (30)$$

$$\Gamma_{A_1 \rightarrow p\bar{p}} = \frac{1}{3\pi} \frac{q_N}{M_{A_1}} (3M_N^2 + 2q_N^2) g_{A_1 pp}^2, \quad (31)$$

$$\Gamma_{S \rightarrow p\bar{p}} = \frac{1}{\pi} \frac{q_N}{M_S^2} (M_N^2 + q_N^2) g_{S pp}^2, \quad (32)$$

which are derived from Eqs. (23), (24), and (29), respectively. Here $q_N = (M_{\Phi, A_1, S}^2 - 4M_N^2)^{1/2}/2$. All the relevant parameters are tabulated in Table. 2. The parameters relevant to $J/\psi \rightarrow \eta_c(1S)\gamma$ are given in Table. 1 for easy comparison.

The scattering amplitudes for the pseudoscalar, axial-vector, and scalar meson exchanges read

$$\mathcal{M}_\Phi^{\mu\nu} = \frac{ie}{M_{J/\psi}} \frac{g_{\gamma\Phi J/\psi} g_{\Phi NN}}{t - M_\Phi^2} e^{\mu\nu\alpha\beta} q_\alpha k_\beta \gamma_5, \quad (33)$$

$$\begin{aligned} \mathcal{M}_{A_1}^{\mu\nu} = & ie \frac{g_{\gamma A_1 J/\psi} g_{A_1 NN}}{t - M_{A_1}^2} e^{\mu\nu\alpha\beta} \left(-g_{\alpha\lambda} + \frac{q_{1\alpha} q_{1\lambda}}{M_{A_1}^2} \right) \\ & \times \left(\gamma^\lambda + \frac{\kappa_{A_1 NN}}{2M_N} \gamma^\sigma \gamma^\lambda q_{1\sigma} \right) \gamma_5 q_\beta, \end{aligned} \quad (34)$$

$$\mathcal{M}_S^{\mu\nu} = -\frac{2e}{M_{J/\psi}} \frac{g_{\gamma S J/\psi} g_{S NN}}{t - M_S^2} (q \cdot k g^{\mu\nu} - q^\mu k^\nu), \quad (35)$$

respectively, where $q_t = k - q$. For the exchanged mesons with finite width Γ_M , the mass is replaced by $M_M \rightarrow (M_M - i\Gamma_M/2)$ in the propagator.

To preserve the unitarity condition, we use the Regge prescription for $\mathcal{M}_{f_1} = \mathcal{M}_{A_1}$ where the Feynman propagator is replaced with the Regge one as

$$\frac{1}{t - M_{f_1}^2} \rightarrow \left(\frac{s}{s_{f_1}}\right)^{\alpha_{f_1}(t)-1} \frac{\pi\alpha'_{f_1}}{\sin[\pi\alpha_{f_1}(t)] \Gamma[\alpha_{f_1}(t)]} D_{f_1}(t). \quad (36)$$

Here $s_{f_1} = 1 \text{ GeV}^2$ and $\alpha_{f_1} = 0.95 + 0.028t$ [52]. The signature factor is in the form of [52]

$$D_{f_1}(t) = \frac{\exp[-i\pi\alpha_{f_1}(t)] - 1}{2}. \quad (37)$$

Each scattering amplitude of Eqs. (33)-(35) is multiplied by the form factor given by

$$F_M(t) = \frac{\Lambda_M^4}{\Lambda_M^4 + (t - M_M^2)^2}, \quad (38)$$

where the cutoff parameters are determined as $(\Lambda_\phi, \Lambda_S, \Lambda_{A_1}) = 2.1 \text{ GeV}$.

3.4. Direct J/ψ radiations

It is found that the direct ϕ radiations play a crucial role in ϕ photoproduction [26, 28, 29]. Thus we include the direct J/ψ radiation term also in J/ψ photoproduction, as drawn in Figs. 3(d,e). The relevant effective Lagrangians are defined by

$$\mathcal{L}_{\gamma NN} = -e\bar{N} \left[\gamma_\mu - \frac{\kappa_N}{2M_N} \sigma_{\mu\nu} \partial^\nu \right] N A^\mu, \quad (39)$$

$$\mathcal{L}_{J/\psi NN} = -g_{J/\psi NN} \bar{N} \left[\gamma_\mu - \frac{\kappa_{J/\psi NN}}{2M_N} \sigma_{\mu\nu} \partial^\nu \right] N \psi^\mu, \quad (40)$$

where the anomalous magnetic moment of the proton is given by $\kappa_p = 1.79$. We set the tensor term of the $J/\psi NN$ vertex to be zero for simplicity. The coupling constant in the vector term is obtained from the branching ratio for $J/\psi \rightarrow p\bar{p}$ and

$$\Gamma_{J/\psi \rightarrow p\bar{p}} = \frac{2}{3\pi} \frac{q_N^3}{M_{J/\psi}^2} g_{J/\psi p\bar{p}}^2, \quad (41)$$

where $q_N = (M_{J/\psi}^2 - 4M_N^2)^{1/2}/2$. From $\Gamma_{J/\psi} = 92.6 \text{ KeV}$ and $\text{Br}_{J/\psi \rightarrow p\bar{p}} = 2.120 \cdot 10^{-3}$ [38], we obtain $|g_{J/\psi NN}| = |g_{J/\psi p\bar{p}}| = 2.18 \cdot 10^{-3}$.

The J/ψ radiation scattering amplitudes for s - and u -channels read

$$\begin{aligned} \mathcal{M}_{J/\psi, \text{rad}, s}^{\mu\nu} &= \frac{eg_{J/\psi NN}}{s - M_N^2} \left(\gamma^\nu - i \frac{\kappa_{J/\psi NN}}{2M_N} \sigma^{\nu\alpha} k_\alpha \right) \\ &\times (q_s + M_N) \left(\gamma^\mu + i \frac{\kappa_N}{2M_N} \sigma^{\mu\beta} q_{s\beta} \right), \end{aligned} \quad (42)$$

$$\begin{aligned} \mathcal{M}_{J/\psi, \text{rad}, u}^{\mu\nu} &= \frac{eg_{J/\psi NN}}{u - M_N^2} \left(\gamma^\mu + i \frac{\kappa_N}{2M_N} \sigma^{\mu\alpha} q_{u\alpha} \right) \\ &\times (q_u + M_N) \left(\gamma^\nu - i \frac{\kappa_{J/\psi NN}}{2M_N} \sigma^{\nu\beta} k_\beta \right), \end{aligned} \quad (43)$$

respectively, where $q_s = q + p_i$ and $q_u = p_f - q$.

We choose the following form factor

$$F_N(\mathbf{k}) = \frac{\Lambda_N^2}{\Lambda_N^2 + \mathbf{k}^2}, \quad (44)$$

to make sure that the integration in calculating the FSI term converges. \mathbf{k} is the 3-momentum of the produced J/ψ meson. The cutoff parameter is chosen to be $\Lambda_N = 2.1 \text{ GeV}$. Note that similar amplitudes are needed for considering the FSI effect through $J/\psi p \rightarrow J/\psi p$ as shown in Figs. 2(b,c) where the same form factor of Eq. (44) will be used.

4. FSI term

The amplitude for the FSI is defined in Eqs. (3)-(6). We keep only the leading term in Eq. (5) which leads to the approximation $t_{J/\psi N, J/\psi N}(E) \sim V_{J/\psi N, J/\psi N}(E)$ in evaluating the FSI amplitude in Eq. (3) such that the individual contributions of $v_{J/\psi N, J/\psi N}^{\text{Gluon}}$ and $v_{J/\psi N, J/\psi N}^{\text{Direct}}$ can be studied. The amplitude $T_{J/\psi N, \gamma N}^{\text{FSI}}(E)$ of Eq. (3) for the reaction of $\gamma(\mathbf{q}) + N(-\mathbf{q}) \rightarrow J/\psi(\mathbf{k}) + N(-\mathbf{k})$ can then be written as

$$\begin{aligned} \langle \mathbf{k} | T_{J/\psi N, \gamma N}^{\text{FSI}}(E) | \mathbf{q} \rangle &= \int d\mathbf{k}' \langle \mathbf{k} | V_{J/\psi N, J/\psi N}(E) | \mathbf{k}' \rangle \\ &\times \frac{1}{E - E_{J/\psi}(k') - E_N(k') + i\epsilon} \langle \mathbf{k}' | B_{J/\psi N, \gamma N} | \mathbf{q} \rangle, \end{aligned} \quad (45)$$

in the c.m. frame.

Now, we need to evaluate the matrix elements of the potential of $V_{J/\psi N, J/\psi N}(E)$ for $J/\psi(k') + N(p') \rightarrow J/\psi(k) + N(p)$, which can be expressed as

$$\begin{aligned} &\langle k\lambda_{J/\psi}; pm_s | V_{J/\psi N, J/\psi N} | k'\lambda'_{J/\psi}; p'm'_s \rangle \\ &= \frac{1}{(2\pi)^3} \sqrt{\frac{M_N^2}{4E_{J/\psi}(\mathbf{k})E_N(\mathbf{p})E_{J/\psi}(\mathbf{k}')E_N(\mathbf{p}')}} \\ &\times \mathcal{V}(k\lambda_{J/\psi}, pm_s; k'\lambda'_{J/\psi}, p'm'_s), \end{aligned} \quad (46)$$

where

$$\mathcal{V} = \mathcal{V}_{\text{Gluon}} + \mathcal{V}_{\text{Direct}}. \quad (47)$$

Here $\mathcal{V}_{\text{Gluon}}$ [Fig. 2(a)] and $\mathcal{V}_{\text{Direct}}$ [Figs. 2(b,c)] represent the gluon-exchange interaction and direct $J/\psi N$ coupling terms, respectively. More details will be followed for these $J/\psi N$ potentials from the interaction Lagrangians by using the unitary transformation method of the ANL-Osaka formulation [39, 40].

4.1. Gluon exchange interaction

Because of the OZI rule, the $J/\psi N$ interaction is expected to be governed by gluon exchanges. Since there exists the LQCD calculations for the $J/\psi N$ potential, we use the form suggested by Ref. [53] for the charmonium-nucleon potential which is found to be approximately of the Yukawa form. We therefore take the form of

$$\mathcal{V}_{\text{Gluon}} = -v_0 \frac{e^{-\alpha r}}{r}, \quad (48)$$

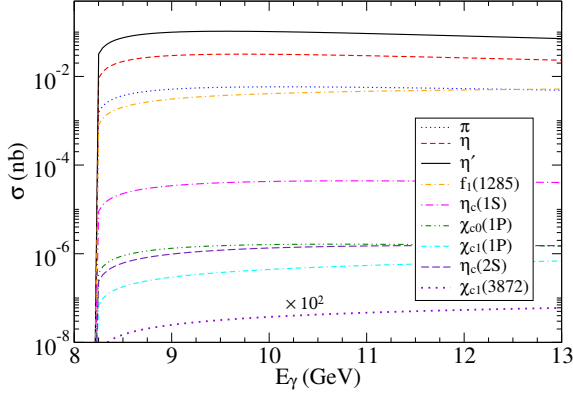


Figure 4: Each contribution of meson exchanges for $\gamma p \rightarrow J/\psi p$ is plotted as a function of the Lab energy E_γ .

which was also adopted in the phenomenological $c\bar{c}$ - N potential [54]. The parameters in Eq. (48) are given by [53, 54]

$$v_0 = 0.1, \quad \alpha = 0.6 \text{ GeV}, \quad (49)$$

$$v_0 = 0.4, \quad \alpha = 0.6 \text{ GeV}. \quad (50)$$

We attempt to use both of them in our calculation and compare the results each other in the next section.

The potential of Eq. (48) can be obtained by taking the non-relativistic limit of the scalar meson exchange amplitude calculated from the Lagrangian

$$\mathcal{L}_\sigma = V_0 (\bar{\psi}_N \psi_N \Phi_\sigma + \psi^\mu \psi_\mu \Phi_\sigma), \quad (51)$$

where Φ_σ is a scalar field with mass α in Eq. (48). By using the unitary transformation method [39, 40], the scalar-meson exchange matrix element derived from Eq. (51) can be written as

$$\mathcal{V}_{\text{Gluon}}(k\lambda_{J/\psi}, pm_s; k'\lambda'_{J/\psi}, p'm'_s) = \frac{V_0}{(p-p')^2 - \alpha^2} \times [\bar{u}_N(p, m_s) u_N(p', m'_s)] [\epsilon_\mu^*(k, \lambda_{J/\psi}) \epsilon^\mu(k', \lambda'_{J/\psi})], \quad (52)$$

where $V_0 = -8v_0\pi M_{J/\psi}$ and $(p-p') = (E_N(p) - E_N(p'), \mathbf{p} - \mathbf{p}')$.

4.2. Direct $J/\psi N$ coupling term

The form of the direct $J/\psi N$ coupling amplitudes is the same as given in Eqs. (42) and (43) after the replacement of e by $g_{J/\psi NN}$ and κ_N by $\kappa_{J/\psi NN}$. We also use the same form of the form factor as given in Eq. (44) and the same cutoff parameter, i.e., $\Lambda_N = 2.1 \text{ GeV}$.

5. Numerical Results and Discussions

5.1. Born term

We first show the results when the Born term is only considered as discussed in Sec. 3. To examine the t -channel meson-exchange mechanism, each contribution of light-meson and charmonium-meson exchanges is displayed in Fig. 4 as a function of the photon Lab energy E_γ . In case of $\eta_c(2S)$ and

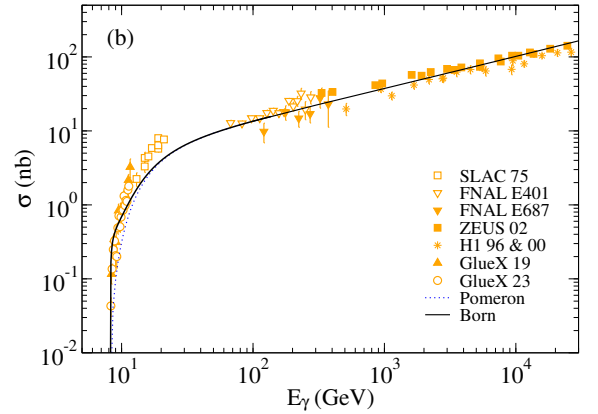
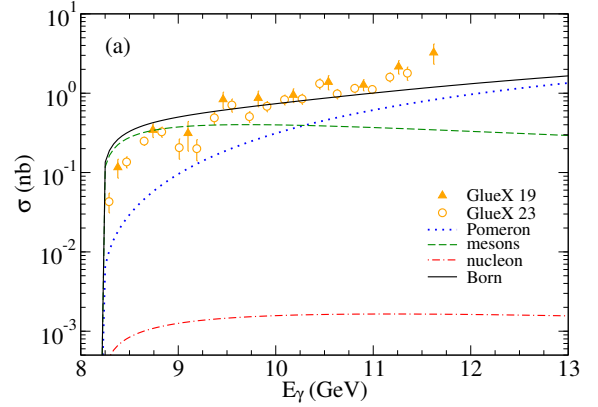


Figure 5: (a) Total cross section for $\gamma p \rightarrow J/\psi p$ without FSI is plotted as a function of the Lab energy E_γ at low energies ($8 \leq E_\gamma \leq 13 \text{ GeV}$). The blue dotted, green dashed, and red dot-dashed curves stand for the contributions of Pomeron, meson, and nucleon exchanges, respectively. The black solid curve denote the Born contribution. (b) Total cross section from threshold up to $E_\gamma \simeq 10^4 \text{ GeV}$. The SLAC [55], FermiLab [2, 3], ZEUS [4], H1 [5, 6], and GlueX [41, 42] data are used.

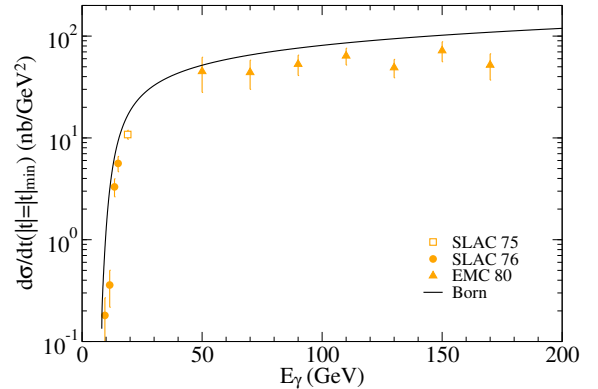


Figure 6: Differential cross section is plotted as a function of the Lab energy E_γ at $|t| = |t_{\text{min}}|$ from threshold up to $E_\gamma = 200 \text{ GeV}$. The SLAC [55, 56] and EMC [57] data are compared with the result from the Born contribution.

$\chi_{c1}(3872)$ mesons, only the upper limits for their branching ratios to $J/\psi\gamma$ or $p\bar{p}$ are provided. Thus their contributions also indicate upper limits on the total cross section. We find that the differences of the cross sections between the light-meson and charmonium-meson contributions are large enough to be dis-

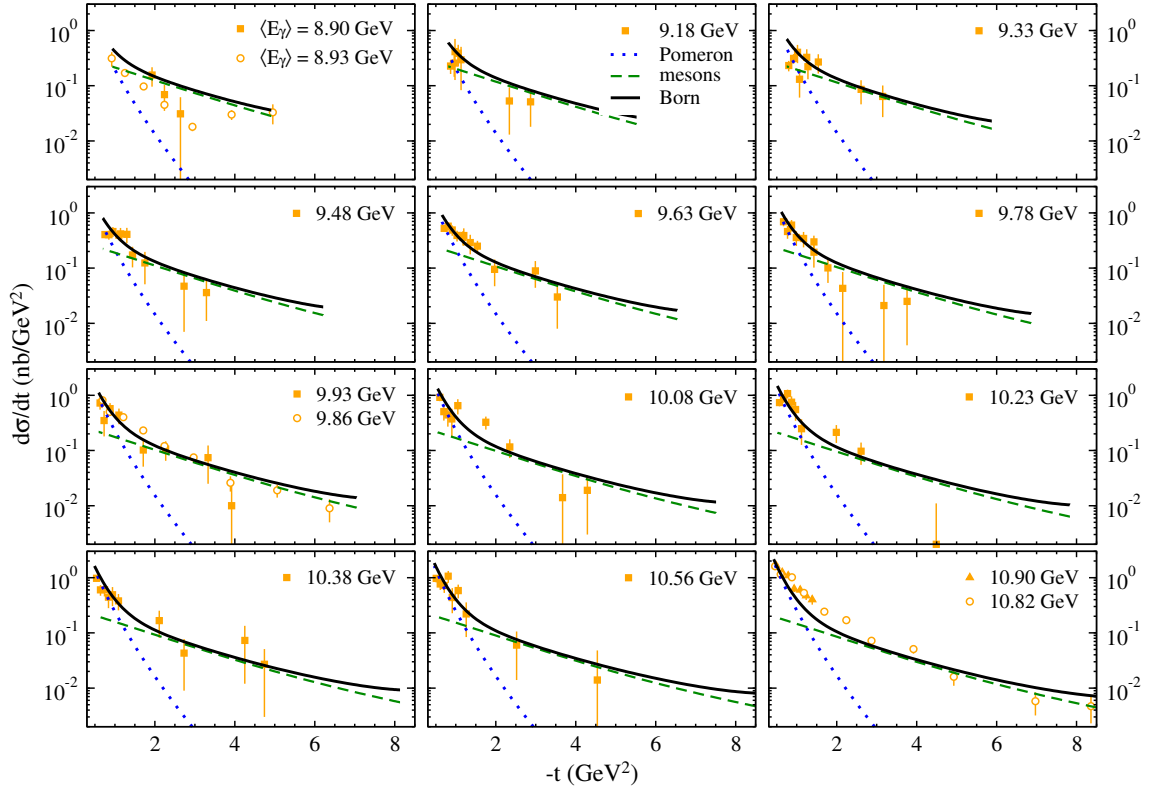


Figure 7: Differential cross sections without FSI are plotted as functions of the momentum transfer $-t$ at different Lab energies ($8.90 \leq E_\gamma \leq 10.90$ GeV). The GlueX19 [41] (triangle), GlueX23 [42] (circle), and J/ψ -007 [43] (quadrangle) data from the JLab are compared with the Pomeron-exchange (blue dotted), meson-exchange (green dashed), and Born (black solid) contributions.

tinguished. Clearly, light mesons make more significant contribution than charmonium mesons. The most dominant contribution from the light- and charmonium-mesons turns out to be $\eta'(958)$ and $\eta_c(1S)$ mesons, respectively. Nevertheless, $\eta_c(1S)$ exchange is about three orders of magnitude suppressed relative to $\eta'(958)$ one.

Figure 5(a) depicts the total cross section of the Born contribution (black solid) which involves the Pomeron exchange (blue dotted) and the sum of meson exchanges (green dashed) shown in Fig. 4. The direct J/ψ -radiation contribution (red dot-dashed) is also given. The results indicate that the contribution of meson exchanges is indeed essential for describing the low-energy GlueX data [41, 42] together with that of Pomeron exchange. Meanwhile, the direct J/ψ -radiation contribution is more suppressed than the meson-exchange one by a factor of about 10^2 . In Fig. 5(b), we show the contributions of the Pomeron exchange and Born term from threshold up to $E_\gamma \approx 10^4$ GeV. The Pomeron exchange describes the high energy data [2, 3, 4, 5, 6, 55] quite well.

In Fig. 6, we present the differential cross section as a function of the Lab energy E_γ at $|t| = |t|_{\min}$. The SLAC [55, 56] and European Muon Collaboration (EMC) [57] data are compared with the result of the Born term. The overall shape of the result is very similar to the available data although the result slightly overestimates the experimental data. Thus our Pomeron model is verified again by this comparison.

Figure 7 displays the results for the differential cross sec-

tions as functions of $-t$. Pomeron exchange alone is insufficient to account for the low energy JLab data [41, 42, 43]. The inclusion of meson exchanges greatly improves the results over the whole scattering angles because the slope of the meson-exchange contribution is very similar to that of the JLab data at $-t \geq 2$ GeV². A similar conclusion is found in ϕ -meson photo-production [26, 28, 29] where light mesons, such as $\pi^0(135)$, $\eta(548)$, $a_0(980)$, $f_0(980)$, and $f_1(1285)$, played an important role for describing the available angle-dependent data [30, 31]. The direct J/ψ -radiation term begins to come into play in the backward scattering regions as expected. That is, because of its contribution, the Born term is increased to some extent in the regions $-t \geq 5$ GeV² in comparison with the meson-exchange term. The GlueX23 data at $E_\gamma = (8.93, 9.86, 10.82)$ GeV [42] cover the whole scattering angles and thus place constraint on the direct J/ψ -radiation contribution.

5.2. FSI term

We are now in a position to show the results with the FSI term where the gluon-exchange interaction and direct J/ψ coupling terms are involved as discussed in Sec. 4. It is found that the contribution of the FSI term entirely comes from the gluon-exchange interaction. Meanwhile the direct J/ψ coupling term is relatively far more suppressed. We attempt to use two different sets of parameters (ν_0, α) as for the Yukawa potential of Eq. (48) in the gluon-exchange interaction: (0.1, 0.6) [53] and (0.4, 0.6) [54], which we call as fit-1 and fit-2 models.

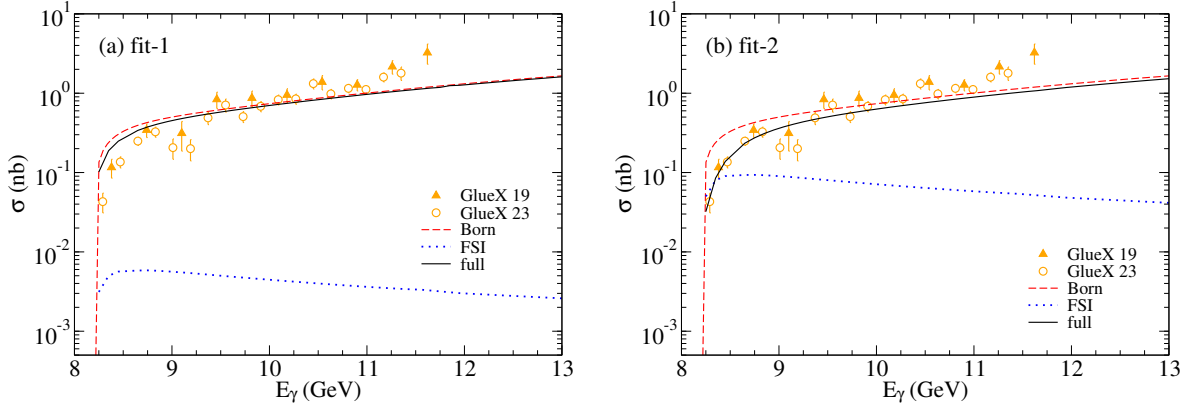


Figure 8: Total cross section for $\gamma p \rightarrow J/\psi p$ with FSI is plotted as a function of the Lab energy E_γ at low energies ($8 \leq E_\gamma \leq 13$ GeV). The red dashed and blue dotted curves stand for the contributions of the Born and FSI terms, respectively. The black solid curve denote the full contribution. The parameters of the Yukawa potential (v_0, α) we have used: (a) fit-1: (0.1, 0.6) [53], (b) fit-2: (0.4, 0.6) [54]. The data are from the GlueX Collaboration [41, 42].

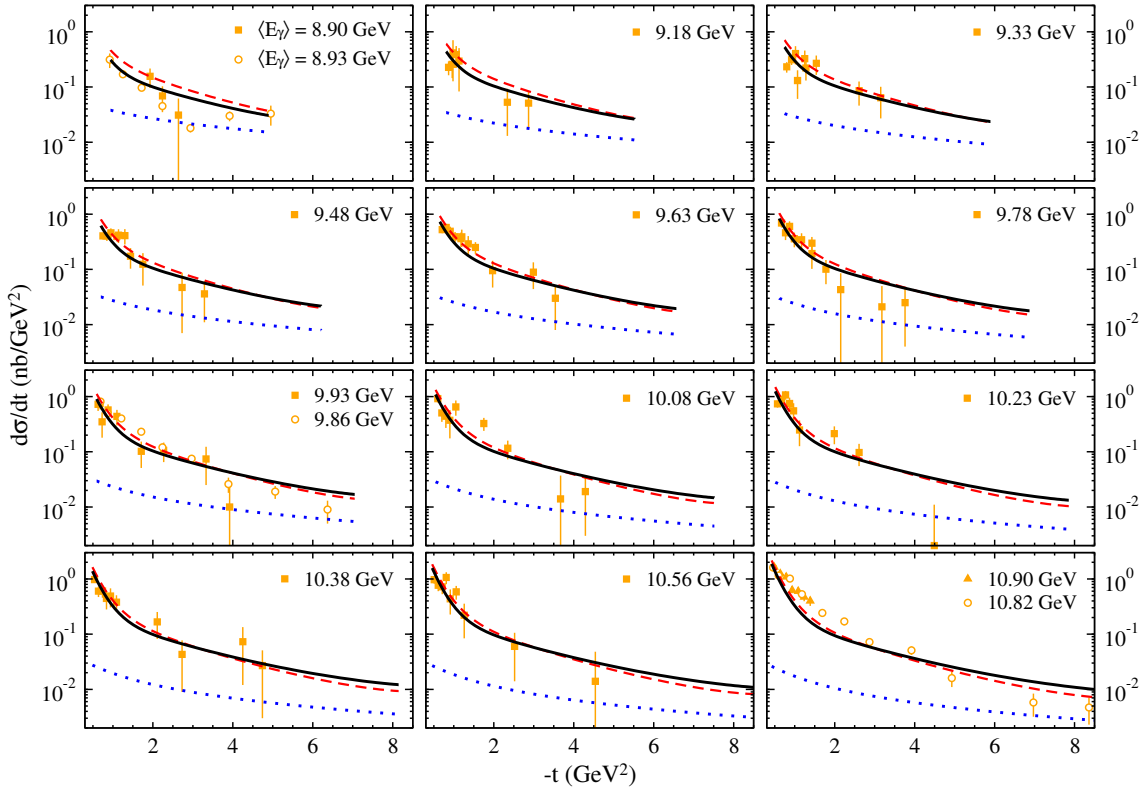


Figure 9: Differential cross sections are plotted as functions of the momentum transfer $-t$ at different Lab energies ($8.90 \leq E_\gamma \leq 10.90$ GeV) with and without the FSI effect. The GlueX19 [41] (triangle), GlueX23 [42] (circle), and J/ψ -007 [43] (quadrangle) data from the JLab are compared with the results with the fit-2 model. The curve notations are the same as those in Fig. 8.

The results for the total cross section with the FSI effect are depicted in Fig. 8 where the red dashed curve (Born term) corresponds to the black solid curve in Fig. 5. It turns out that the the Born term interferes destructively with the FSI term. The FSI effect is small when we use the fit-1 model (Fig. 8(a)) but is significant when the fit-2 model is used (Fig. 8(b)). Indeed, we find a noticeable improvement with the fit-2 model near the threshold.

The differential cross sections corresponding to the fit-2

model are displayed in Fig. 9 as functions of $-t$. The contribution of the FSI term is about $10^1 - 10^2$ times smaller than that of the Born term depending on the kinematical regions. The Born term interferes destructively with the FSI term at forward scattering angles ($-t \leq 4$ GeV²) and interferes constructively at backward scattering angles ($-t \geq 4$ GeV²). The FSI term makes the result much better at $E_\gamma = 8.93$ GeV in particular. More accurate angle-dependent data near the very threshold ($E_\gamma \leq 8.9$ GeV) are strongly desired to verify the role of the

FSI term. Note that both the direct J/ψ -radiation term in Born amplitude and the FSI term enhance the results in the backward scattering regions ($-t \geq 4 \text{ GeV}^2$).

6. Summary and Conclusion

In this letter, we aimed at investigating J/ψ -meson photoproduction off the nucleon target within a dynamical model approach based on a Hamiltonian [39, 40] which can generate the $\gamma N \rightarrow J/\psi N$ reaction and $J/\psi N \rightarrow J/\psi N$ FSI term. The Born amplitude for $\gamma p \rightarrow J/\psi p$ consists of the Pomeron exchange, meson exchanges in the t channel, and direct J/ψ radiations in the s - and u -channels.

The role of light-meson and charmonium-meson exchanges is extensively studied and the relevant electromagnetic coupling constants involved in the effective Lagrangians are determined by the radiative decays of J/ψ and charmonium mesons [38]. Meanwhile, the meson- NN coupling constants are taken from the Nijmegen potentials and radiative decays of charmonium mesons to $p\bar{p}$ for the light- and charmonium-meson exchanges, respectively. We have found that $\eta(548)$ and $\eta'(958)$ light mesons play a crucial role to describe the available JLab data [41, 42, 43] but charmonium mesons give a negligible contribution to the $\gamma p \rightarrow J/\psi p$ reaction.

The final J/ψ - N interaction is required by the unitarity condition and the Yukawa form of $[-v_0 \exp(-\alpha r)/r]$ is assumed as for the charmonium-nucleon potential when considering the gluon-exchange interaction. To check the model dependence of the FSI effect, two different sets of parameters are attempted [53, 54]. The FSI effect turned out to be essential to account for the threshold region when the values of $(v_0, \alpha) = (0.4, 0.6)$ [54] are used. Note that the importance of the FSI effect is also found in Ref. [58] where a model based on the constituent quark model (CQM) and a phenomenological charm quark-nucleon potential is constructed to investigate the $\gamma p \rightarrow J/\psi p$ reaction. Meanwhile, the author and his collaborators have found that the FSI effect is small in ϕ -meson photoproduction where a similar dynamical approach is employed [28].

Our reaction model provides an excellent description of the total and t -dependent differential cross sections and can be justified after more high-precision angle-dependent data are accumulated near the very threshold ($E_\gamma \leq 8.9 \text{ GeV}$). Also the measurements of various spin polarization observables by future experiments will become valuable information for a better understanding of the J/ψ photoproduction mechanism.

Acknowledgments

The author is grateful to T.-S. H. Lee and S.-i. Nam for valuable discussions. The work was supported by the Basic Science Research Program through the National Research Foundation of Korea (NRF) under Grants No. RS-2021-NR060129 and No. RS-2022-NR074739.

References

- [1] J. M. Laget, Photoproduction of vector mesons at large transfer, *Phys. Lett. B* **489** (2000) 313.
- [2] M. E. Binkley, *et al.*, J/ψ photoproduction from 60 to 300 GeV/c, *Phys. Rev. Lett.* **48** (1982) 73.
- [3] P. L. Frabetti, *et al.*, A measurement of elastic J/ψ photoproduction cross section at Fermilab E687, *Phys. Lett. B* **316** (1993) 197.
- [4] ZEUS Collaboration, Exclusive photoproduction of J/ψ mesons at HERA, *Eur. Phys. J. C* **24** (2002) 345.
- [5] H1 Collaboration, Elastic and inelastic photoproduction of J/ψ mesons at HERA, *Nucl. Phys. B* **472** (1996) 3.
- [6] H1 Collaboration, Elastic photoproduction of J/ψ and Υ mesons at HERA, *Phys. Lett. B* **483** (2000) 23.
- [7] A. Donnachie and P. V. Landshoff, Small x : Two pomerons!, *Phys. Lett. B* **437** (1998) 408.
- [8] A. Donnachie and P. V. Landshoff, Charm production at HERA, *Phys. Lett. B* **470** (1999) 243.
- [9] A. Donnachie and P. V. Landshoff, Exclusive vector photoproduction: Confirmation of Regge theory, *Phys. Lett. B* **478** (2000) 146.
- [10] A. Donnachie and P. V. Landshoff, New data and the hard Pomeron, *Phys. Lett. B* **518** (2001) 63.
- [11] T.-S. H. Lee, S. Sakinah, and Y. Oh, Models of J/ψ photo-production reactions on the nucleon, *Eur. Phys. J. A* **58** (2022) 252.
- [12] S. J. Brodsky, E. Chudakov, P. Hoyer, and J. M. Laget, Photoproduction of charm near threshold, *Phys. Lett. B* **498** (2001) 23.
- [13] Y. Guo, X. Ji, and Y. Liu, QCD Analysis of near-threshold photon-proton production of heavy quarkonium, *Phys. Rev. D* **103** (2021) 096010.
- [14] K. A. Mamo and I. Zahed, Diffractive photoproduction of J/ψ and Υ using holographic QCD: Gravitational form factors and GPD of gluons in the proton, *Phys. Rev. D* **101** (2020) 086003.
- [15] K. A. Mamo and I. Zahed, Electroproduction of heavy vector mesons using holographic QCD: From near threshold to high energy regimes, *Phys. Rev. D* **104** (2021) 066023.
- [16] Q. Wang, X. H. Liu, and Q. Zhao, Photoproduction of hidden charm pentaquark states $P_c^+(4380)$ and $P_c^+(4450)$, *Phys. Rev. D* **92** (2015) 034022.
- [17] V. Kubarovsky and M. B. Voloshin, Formation of hidden-charm pentaquarks in photon-nucleon collisions, *Phys. Rev. D* **92** (2015) 031502.
- [18] M. Karliner and J. L. Rosner, Photoproduction of exotic baryon resonances, *Phys. Lett. B* **752** (2016) 329.
- [19] A. N. Hiller Blin, C. Fernández-Ramírez, A. Jackura, V. Mathieu, V. I. Mokeev, A. Pilloni, and A. P. Szczepaniak, Studying the $P_c(4450)$ resonance in J/ψ photoproduction off protons, *Phys. Rev. D* **94** (2016) 034002.
- [20] X. Y. Wang, X. R. Chen, and J. He, Possibility to study pentaquark states $P_c(4312)$, $P_c(4440)$, and $P_c(4457)$ in $\gamma p \rightarrow J/\psi p$ reaction, *Phys. Rev. D* **99** (2019) 114007.
- [21] J. J. Wu, T. S. H. Lee, and B. S. Zou, Nucleon resonances with hidden charm in γp reactions, *Phys. Rev. C* **100** (2019) 035206.
- [22] D. Winney, *et al.* (Joint Physics Analysis Center), Double polarization observables in pentaquark photoproduction, *Phys. Rev. D* **100** (2019) 034019.
- [23] D. Winney, *et al.* (Joint Physics Analysis Center), Dynamics in near-threshold J/ψ photoproduction, *Phys. Rev. D* **108** (2023) 054018.
- [24] LHCb Collaboration, Observation of $J/\psi p$ resonances consistent with pentaquark states in $\Lambda_b^0 \rightarrow J/\psi K^- p$ decays, *Phys. Rev. Lett.* **115** (2015) 072001.
- [25] LHCb Collaboration, Observation of a narrow pentaquark state, $P_c(4312)^+$, and of two-peak structure of the $P_c(4450)^+$, *Phys. Rev. Lett.* **122** (2019) 222001.
- [26] S. H. Kim and S.-i. Nam, Pomeron, nucleon-resonance, and $(0^+, 0^-, 1^+)$ -meson contributions in ϕ -meson photoproduction, *Phys. Rev. C* **100** (2019) 065208.
- [27] S. H. Kim and S.-i. Nam, Investigation of electroproduction of ϕ mesons off protons, *Phys. Rev. C* **101** (2020) 065201.
- [28] S. H. Kim, T.-S. H. Lee, S.-i. Nam, and Y. Oh, Dynamical model of ϕ meson photoproduction on the nucleon and ^4He , *Phys. Rev. C* **104** (2021) 045202.
- [29] S. H. Kim, T.-S. H. Lee, S.-i. Nam, and Y. Oh, ϕ meson photoproduction on the nucleon and ^4He targets, *Few Body Syst.* **65** (2024) 19.
- [30] CLAS Collaboration, ϕ -meson photoproduction on hydrogen in the neutral decay mode, *Phys. Rev. C* **89** (2014) 055206.

- [31] CLAS Collaboration, Data analysis techniques, differential cross sections, and spin density matrix elements for the reaction $\gamma p \rightarrow \phi p$, *Phys. Rev. C* **89** (2014) 055208; **90** (2014) 019901(E).
- [32] CLAS Collaboration, Exclusive electroproduction of ϕ mesons at 4.2 GeV, *Phys. Rev. C* **63** (2001) 065205; **64** (2001) 059901(E).
- [33] CLAS Collaboration, Electroproduction of $\phi(1020)$ mesons at $1.4 \leq Q^2 \leq 3.8$ GeV² measured with the CLAS spectrometer, *Phys. Rev. C* **78** (2008) 025210.
- [34] LEPS Collaboration, Measurement of spin-density matrix elements for ϕ -meson photoproduction from protons and deuterons near threshold, *Phys. Rev. C* **82** (2010) 015205.
- [35] S. Okubo, Phi meson and unitary symmetry model, *Phys. Lett.* **5** (1963) 165.
- [36] G. Zweig, CERN Reports, CERN-TH-401 and CERN-TH-412, 1964.
- [37] J. Iizuka, Systematics and phenomenology of meson family, *Prog. Theor. Phys. Suppl.* **37** (1966) 21.
- [38] S. Navas, *et al.*, Particle Data Group, *Phys. Rev. D* **110** (2024) 030001.
- [39] A. Matsuyama, T. Sato, and T. S. H. Lee, Dynamical coupled-channel model of meson production reactions in the nucleon resonance region, *Phys. Rept.* **439** (2007) 193.
- [40] H. Kamano, T.-S. H. Lee, S. X. Nakamura, and T. Sato, The ANL-Osaka partial-wave amplitudes of πN and γN reactions, [arXiv:1909.11935](https://arxiv.org/abs/1909.11935) [nucl-th].
- [41] GlueX Collaboration, First measurement of near-threshold J/ψ exclusive photoproduction off the proton, *Phys. Rev. Lett.* **123** (2019) 072001.
- [42] GlueX Collaboration, Measurement of the J/ψ photoproduction cross section over the full near-threshold kinematic region, *Phys. Rev. C* **108** (2023) 025201.
- [43] B. Duran, *et al.*, Determining the gluonic gravitational form factors of the proton, *Nature* **615** (2023) 813.
- [44] A. Donnachie and P. V. Landshoff, Elastic scattering and diffraction dissociation, *Nucl. Phys. B* **244** (1984) 322.
- [45] A. Donnachie and P. V. Landshoff, Dynamics of elastic scattering, *Nucl. Phys. B* **267** (1986) 690.
- [46] A. Donnachie and P. V. Landshoff, Exclusive rho production in deep inelastic scattering, *Phys. Lett. B* **185** (1987) 403.
- [47] S. R. Beane, E. Chang, S. D. Cohen, W. Detmold, H. W. Lin, K. Orginos, A. Parreño, and M. J. Savage, Quarkonium-nucleus bound states from Lattice QCD, *Phys. Rev. D* **91** (2015) 114503.
- [48] M. L. Goldberger and K. M. Watson, *Collision Theory* (John Wiley and Sons, Inc., New York, 1964).
- [49] V. G. J. Stoks and Th. A. Rijken, Soft-core baryon-baryon potentials for the complete baryon octet, *Phys. Rev. C* **59** (1999) 3009.
- [50] Th. A. Rijken, V. G. J. Stoks, and Y. Yamamoto, Soft-core hyperon-nucleon potentials, *Phys. Rev. C* **59** (1999) 21.
- [51] M. Birkel and H. Fritzsche, Nucleon spin and the mixing of axial vector mesons, *Phys. Rev. D* **53** (1996) 6195.
- [52] N. I. Kochelev, D. P. Min, Y. Oh, V. Vento, and A. V. Vinnikov, New anomalous trajectory in Regge theory, *Phys. Rev. D* **61** (2000) 094008.
- [53] T. Kawanai and S. Sasaki, Charmonium-nucleon potential from lattice QCD, *Phys. Rev. D* **82** (2010) 091501.
- [54] S. J. Brodsky, I. A. Schmidt, and G. F. de Teramond, Nuclear bound quarkonium, *Phys. Rev. Lett.* **64** (1990) 1011.
- [55] U. Camerini, J. G. Learned, R. Prepost, C. M. Spencer, D. E. Wiser, W. Ash, R. L. Anderson, D. Ritson, D. Sherden, and C. K. Sinclair, Photoproduction of the ψ Particles, *Phys. Rev. Lett.* **35** (1975) 483.
- [56] D. M. Ritson, ψ and excess leptons in photoproduction, *AIP Conf. Proc.* **30** (1976) 75.
- [57] European Muon Collaboration, Measurement of J/ψ production in 280-GeV/c μ^+ iron interactions, *Phys. Lett. B* **89** (1980) 267.
- [58] S. Sakinah, T. S. H. Lee, and H. M. Choi, Dynamical model of J/ψ photoproduction on the nucleon, *Phys. Rev. C* **109** (2024) 065204.